Title
Structural and Na-ion conduction characteristics of Na 3 PS x Se 4−x

Journal
Journal of Materials Chemistry A, 4(23)

ISSN
2050-7488

Authors
Bo, Shou-Hang
Wang, Yan
Ceder, Gerbrand

Publication Date
2016

DOI
10.1039/c6ta03027k

Peer reviewed

Structural and Na-ion conduction characteristics of $Na_3PS_xSe_{4-x}$

Shou-Hang Bo[a,b], Yan Wang[a] and Gerbrand Ceder[a,b,c*]

[a] Department of Materials Science and Engineering, Massachusetts Institute of Technology, Cambridge, MA 02139, United States

[b] Materials Science Division, Lawrence Berkeley National Laboratory, Berkeley, CA 94720, United States

[c] Department of Materials Science and Engineering, University of California, Berkeley, CA 94720, United States

Corresponding Author: gceder@berkeley.edu

Abstract:

The recent discovery of the isostructrual cubic Na_3PS_4 and Na_3PSe_4 as fast Na-ion conductors provided a general structural framework for the exploration of new sodium superionic conductors. In this work, we systematically investigated the structures and ionic conduction characteristics of a series of compounds with the general chemical formula of $Na_3PS_xSe_{4-x}$. Synthesis of Na_3PS_4 at different conditions (*e.g.*, temperature, reaction vessel, mass of the precursors) reveals the reactivity of the precursors with the reaction tubes, producing different polymorphs. X-ray diffraction studies on the solid solution phases $Na_3PS_xSe_{4-x}$ identified a tetragonal-to-cubic phase transition with increasing Se concentration. This observation is consistent with the computed stability of the tetragonal and cubic polymorphs, where the energy difference between the two polymorphs becomes very close to zero in Se-rich compositions. Furthermore, *ab initio* molecular dynamic simulations suggest that the fast Na-ion conduction in $Na_3PS_xSe_{4-x}$ may not be causally related with the symmetry or the composition of these phases. The formation of defects, instead, enables fast Na-ion conduction in this class of materials.

Introduction

The potential hazards associated with the liquid electrolyte in rechargeable batteries (*e.g.*, leakage and flammability) are one of the major hurdles preventing the widespread application of batteries in large-scale devices, such as electric vehicles. Replacing the liquid electrolyte with an inflammable solid state electrolyte can, in principle, eliminate the safety concerns, offering a promising path forward to extend the application of batteries to devices where safety is of uttermost importance. The development of fast Na-ion conductors as solid state electrolytes is a key enabler for an all-solid-state Na-ion battery technology, which can be less expensive than its Li counterpart due to the wider availability of Na resources and broader choice of Na-intercalation cathodes [1-6]. However, few Na-ion solid state conductors with conductivity approaching that of liquid electrolytes currently exist[7-10]. These considerations motivated us to explore new fast Na-ion conductors, which resulted in our recent investigations on $Na_{10}SnP_2S_{12}$ [11] and cubic Na_3PSe_4[12].

Cubic Na_3PSe_4 is isostructral to cubic Na_3PS_4 [12-15]. Both phases crystallize in the *I-43m* (#217) space group. The lattice parameter of the Se compound is approximately 4% larger than that of the S compound, due to the larger ionic radius of Se^{2-} (the ionic radii of Se^{2-} and S^{2-} in Å are 1.98 and 1.84, respectively). The close similarity between Na_3PS_4 and Na_3PSe_4 implies that a solid solution between these two end members may form, which could provide an effective means to adjust the physical/chemical properties of the $Na_3PS_xSe_{4-x}$ compounds. Indeed, in a very recent paper, the syntheses of $Na_3PS_{0.5}Se_{3.5}$ and $Na_3PS_2Se_2$ were reported, although neither diffraction patterns nor structural parameters were reported in that work [14].

The PX_4^{3-} (X= S, Se) groups in cubic Na_3PX_4 adopt a *body-centered-cubic* (*bcc*) arrangement, with the Na cations occupying the tetrahedral cavities formed by the X^{2-} anions. Such *bcc* anion (or polyanion) arrangements were recently suggested to be beneficial to high intrinsic cation mobility [16]. Indeed, previous impedance measurements showed that cubic Na_3PS_4 and Na_3PSe_4 exhibit high conductivity at room temperature (0.1-1.0 mS/cm), and low activation energies for Na^+ diffusion (20-30 kJ/mol) [12-14]. However, our previous computational investigation on cubic Na_3PSe_4 indicates that the defect-free structure does not permit rapid Na-ion diffusion[12]. This result can also be understood on the basis of crystal structure analysis. The Na in the activated tetrahedral site is only 1.8 Å away from the neighboring Na ion, which is even smaller than the ionic diameter of Na^+ (~ 2.0 Å). This unfavorable interaction makes Na^+ hopping into a transient site energetically unfavorable. In a very recent computational study, Ong and co-workers similarly found that the isostructural cubic Na_3PS_4 without any defect is an extremely poor Na-ion conductor[17]. When a small amount of interstitial Na or Na vacancies are introduced in the calculations, both cubic Na_3PS_4 and Na_3PSe_4 can be shown to have very low Na^+ migration barriers [12,17]. These prior studies suggest that the presence of defects (*e.g.*, Na vacancy, Na interstitial, or Frenkel defect) is essential to enable fast Na-ion diffusion, and highlight the critical importance to understand defect chemistry in Na_3PX_4.

Ab initio DFT calculations indicate that the ground-state structure of Na_3PX_4 (X= S, Se) at 0 K is tetragonal, and not cubic[12, 17]. Small structural differences exist between these two polymorphs, as reflected in the orientation of the PX_4^{3-} tetrahedra, Na cation distribution, and lattice dimensions (Fig. 1). The stabilization mechanism of the metastable cubic Na_3PX_4 phases is not yet clear. While it is possible that entropy stabilizes the cubic phases at elevated temperatures, the tetragonal phase is likely to be re-formed at room temperature, since a

transformation between the cubic and tetragonal polymorphs only requires a slight rotation of the PS_4^{3-} tetrahedra and the re-distribution of Na ions, both of which are expected to be facile in this fast Na-ion conductor. It is, therefore, interesting to investigate more broadly the stabilization mechanism of cubic Na_3PX_4, which could provide valuable insights into future materials design and optimization.

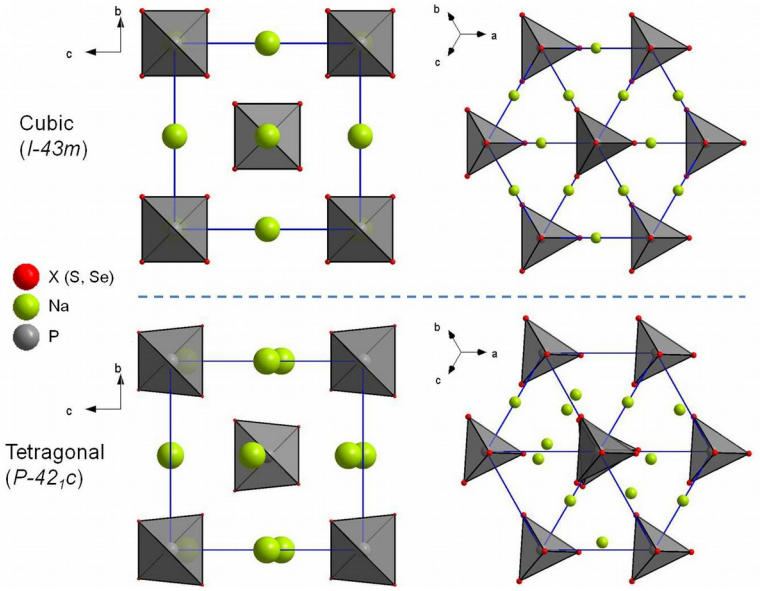

Figure 1. Crystal structures of the cubic (top) and tetragonal (bottom) Na_3PX_4 (X = S, Se). The structures are viewed along the [100] and [111] lattice directions to emphasize the difference between these two polymorphs in terms of Na-ion distribution and PX_4^{3-} tetrahedra orientation.

The two polymorphs of Na_3PS_4 (*i.e.*, tetragonal and cubic) exhibit substantially different ionic conduction behavior. While the cubic phase is one of the fastest Na-ion conductors discovered to date[13], the tetragonal phase is a very poor conductor[18]. These results might be taken to indicate that fast Na-ion conduction is causally related with the symmetry of Na_3PS_4. However, based on our calculations as will be discussed below, this may not be the case.

In the following discussion, we first articulate the effect of synthesis conditions on the structure of Na_3PS_4, since these results provide important insights into the stabilization mechanism of the metastable cubic polymorph. Then, we describe the structures and the Na-ion conduction characteristics of the $Na_3PS_xSe_{4-x}$ phases. The manuscript is concluded with a discussion of the link between crystal structure, defect formation and Na-ion conduction in $Na_3PS_xSe_{4-x}$.

Methods

Synthesis of $Na_3PS_4Se_{4-x}$: Na_2Se (Alfa Aesar, 99.8%), Na_2S (Sigma Aldrich), red phosphorus (Sigma Aldrich, ≥99.99% trace metal basis), selenium (Sigma Aldrich, 99.99% trace metal basis) and sulfur (Sigma Aldrich, 99.998% trace metal basis) powder were used as precursors to produce $Na_3PS_xSe_{4-x}$. These precursors were mixed in an Argon filled glove box according to the target compositions. The resulting mixture (typically ~1 g) was then placed into a BN tube (3 mm inner diameter and 4 mm outer diameter), which was wrapped in aluminum foil, with the open end sealed with a stainless steel Swagelok cap (3/8 inch). This tube was transferred into a sealed alumina tube furnace, which was purged with pre-dried Ar gas (oxygen/moisture traps, model MT200-4-D, Agilent). The furnace was quickly ramped to 300 °C within ~10 minutes, and was held at the same temperature for 12 h to complete the reaction. During the reaction, a continuous flow of Argon gas with a flow rate of approximately 30 mL min^{-1} was used. Final products were collected after the furnace was naturally cooled down to room temperature, and were transferred immediately into the glove box. The $Na_3PS_xSe_{4-x}$ powder was manually ground and re-heated with the same condition to obtain the final product. To test

the impact of synthesis conditions on the structures of Na_3PS_4, additional syntheses of Na_3PS_4 were performed with the use of different reaction vessels, at different temperatures, and with different amounts of precursors.

Experimental characterization: To verify the phase purity of the as-prepared $Na_3PS_xSe_{4-x}$ samples, X-ray diffraction was performed on a Rigaku Smartlab diffractometer with Cu K_α radiation. Typically, the powder sample was first sealed into a special glass capillary (0.5 mm in diameter, Charles Supper) in the glove box, and was then measured in the diffractometer equipped with a capillary stage. We utilized convergent beam and a 1D silicon strip detector (*i.e.*, D/tex Ultra high speed detector) to improve the signal-to-noise ratio of the diffraction data. For structural determination of $Na_3PS_xSe_{4-x}$, the diffraction data was collected at beamline 11BM at the Advanced Photon Source (APS) of Argonne National Laboratory with a constant wavelength of ~0.41 Å. Due to the air sensitivity of $Na_3PS_xSe_{4-x}$ samples, the as-prepared $Na_3PS_xSe_{4-x}$ powder was packed into a 0.5-mm diameter special glass capillary in an argon glove box. The glass capillary was further secured into a 0.8-mm diameter Kapton tube. The Rietveld refinements were performed using the TOPAS 4.2 software package (Bruker).

Impedance measurements of $Na_3PS_xSe_{4-x}$ were performed with a Solartron MTS system. The impedance data were collected from 1 MHz to 100 Hz with a *dc* voltage amplitude of 10 mV. To prepare the sample for impedance measurements, 80-100 mg of $Na_3PS_xSe_{4-x}$ powder was first pressed into a disk-shaped pellet with the use of a 1/4 inch die under a pressure of 1-1.2 metric tons. Indium metal disks (99.999%, Goodfellow Corporation) were then pressed onto both sides of the pellet with a pressure of approximately 0.8 metric tons. The resulting pellet was assembled into a Swagelok cell, using stainless steel rods as current collectors. The Swagelok cell was subsequently sealed into a tube furnace under a continuous flow of Ar for variable

temperature impedance measurements. Data were collected from room temperature to approximately 100 °C during both the heating and cooling cycles.

First-principles density-functional-theory calculations: We performed calculations using density functional theory (DFT) based on the Perdew-Burke-Ernzerhof generalized gradient approximation [19] with interactions between ion cores and valence electrons described by the projector augmented wave method [20] as implemented in the VASP package [21]. A plane-wave energy cut-off of 520 eV and *k*-point density of at least 500/(number of atoms in the unit cell) was used for total energy calculations.

Thermodynamic stability was evaluated using computed DFT total energies. The stability of any phase was evaluated by comparing its energy to linear combinations of the energy of other phases (leading to the same composition) using the convex hull construction. The stability analysis was performed versus all compounds present in the International Crystal Structure Database (ICSD) database [22] plus our internal database of predicted compounds generated with data-mined substitution rules [23]. All unary, binary and ternary compounds in the given Na−P−X system (X = S or Se) were calculated. The stability was quantified by evaluating the energy above the hull, which represents the magnitude of a compound's decomposition energy. A non-negative value of the energy above the hull measures the thermodynamic driving force for the compound to decompose into a set of alternate phases. A thermodynamically stable compound should have 0 meV/atom above the hull as it is part of the convex hull of stable phases.

Gamma-point only sampling of *k*-space and a plane-wave energy cutoff of 400 eV were used for the *ab-initio* Molecular dynamics (AIMD) simulations. The Na_3PX_4 (X=S, Se) supercell consists of 16 formula units. About 2.1% of Na vacancies are introduced in the AIMD

simulations (one Na ion is removed from the supercell originally containing 48 Na ions). The AIMD simulations were preformed in the canonical ensemble with a time step of 2 femtosecond. Temperatures were initialized at 100K and elevated to appropriate temperatures (500K, 600 K, 720K, 900 K and 1200 K). Statistical analysis of the AIMD simulations was performed on 80 ~ 160 picoseconds. The diffusivities of Na ions were calculated from the Na atomic trajectories.

To calculate the Na vacancy formation energy, a charge-neutral Na atom is removed from a supercell with the same size as those used in the AIMD simulation. The defect formation energy of Na_3PX_4 (X=S, Se) is obtained as [24]:

$$E_d = E_{pristine} - E_{defect} + \mu_{Na}$$

where E_{defect} and $E_{pristine}$ are the total energy of the supercell with and without the defect, respectively, and μ_{Na} is the chemical potential of element Na. The Na chemical potential was determined from the multi-phase equilibrium that contains the composition of the defect structure, and was calculated as the slope in the direction of elemental Na in the phase diagram. The python materials genomics (pymatgen) open-source library [25] was used to generate the phase diagram and calculate the chemical potentials. Phase diagrams were constructed by calculating all relevant structures from the ICSD, and from our internal database of structures generated with data-mined substitution rules.

Results

Synthesis of cubic Na_3PS_4

In our attempts to produce cubic Na_3PS_4, we observed that the formation of cubic Na_3PS_4 depends on the synthesis temperature, the type of the reaction vessel, and the mass of the precursors. The synthesis of Na_3PS_4 was first performed by placing the Na_2S and P_2S_5 powder mixture (approximately 0.1 g) into a quartz tube. Fig. 2 presents the X-ray diffraction patterns of the Na_3PS_4 products prepared at different temperatures ranging from 300 °C to 700 °C. The tetragonal and cubic polymorphs of Na_3PS_4 can be distinguished by the characteristic peak splitting associated with the tetragonal structure. For instance, the tetragonal Na_3PS_4 exhibits two well-defined peaks (022_t and 220_t, where "t" is used to denote the tetragonal symmetry) at approximately 36.5° (2θ) as shown in the diffraction data of the sample prepared at 300 °C (Fig. 2b). The cubic phase, on the other hand, shows only one 022_c reflection (where "c" denotes the cubic symmetry) in the same angle range (Fig. 2b, 500 °C sample). This difference between the cubic and tetragonal phases can be understood from the lattice parameters of the cubic and tetragonal lattices. When *a* and *b* are different from *c*, as in tetragonal symmetry, the *022* and *220* peaks are not equivalent. These two peaks (or peaks with similar *hkl*s) become degenerate in cubic symmetry, where *a*, *b* and *c* are equal. Depending on the degree of tetragonal distortion and the $\Delta d/d$ resolution of the diffraction measurements, the peak splitting associated with tetragonal lattices may also appear as peak asymmetry. This is clearly observed in the diffraction data of the two samples prepared at 600 °C and 700 °C. While the cubic phase (500 °C sample) exhibits only one reflection at ~56°, the tetragonal phase (600 and 700 °C samples) shows one peak with asymmetry toward lower angle (Fig. 2b). It is intriguing to note that the cubic Na_3PS_4 only forms at approximately 500 °C. At synthesis temperatures below 500 °C, Na_3PS_4 forms as a tetragonal

polymorph consistent with prior literature [18]. Above 500 °C, another tetragonal polymorph is formed (Fig. 3). Compared with the room-temperature tetragonal phase, the diffraction pattern of this phase can be indexed with the same space group (i.e., *P-42$_1$c*), but the lattices parameters are closer to those of the cubic polymorph (Fig. 3).

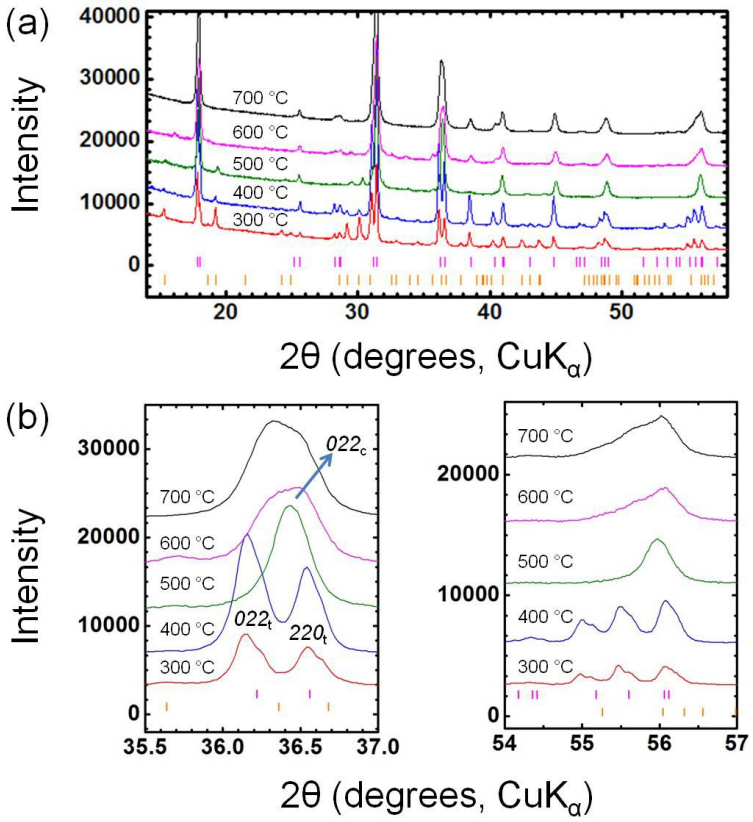

Figure 2. X-ray diffraction patterns of Na_3PS_4 synthesized at different temperatures are shown in (a). An enlarged view of the data from 35.5 to 37.0°, and from 54 to 57° is shown in (b). *022*$_t$, *220*$_t$ and *022*$_c$ reflections are marked on the figure, with the letter "t" and "c" denoting the tetragonal and cubic symmetry of the lattices, respectively. Na_3POS_3 was observed as one of the major impurities. The diffraction peaks corresponding to the tetragonal Na_3PS_4 are marked with magenta tick marks, and the tick marks for peaks corresponding to Na_3POS_3 are shown in dark yellow.

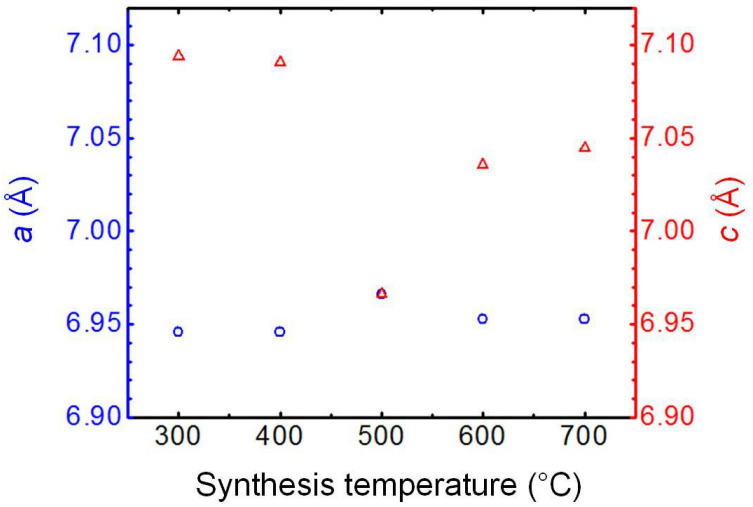

Figure 3. Lattice parameters of Na_3PS_4 samples prepared at different temperatures. The blue circles denote cell dimension along the *a* (or *b*) direction, and the red triangles denote that of the *c* direction.

As 500 °C appears to be the optimal temperature to prepare the cubic phase, we have evaluated the effect of the reaction vessels on the synthesis products. Six different types of tubes, made of quartz, aluminum, vanadium, boron nitride, gold and tantalum were used. The low-temperature tetragonal Na_3PS_4 was obtained when using boron nitride or gold tubes (Fig. 4), the medium-temperature cubic Na_3PS_4 was produced when using quartz, aluminum or tantulum tubes, and the high-temperature tetragonal Na_3PS_4 was obtained when using vanadium tubes. It is worth noting that when the gold tube was used, we observed the formation of Na_3AuS_2 as a side product, highlighting the reactivity of the sulfides with gold.

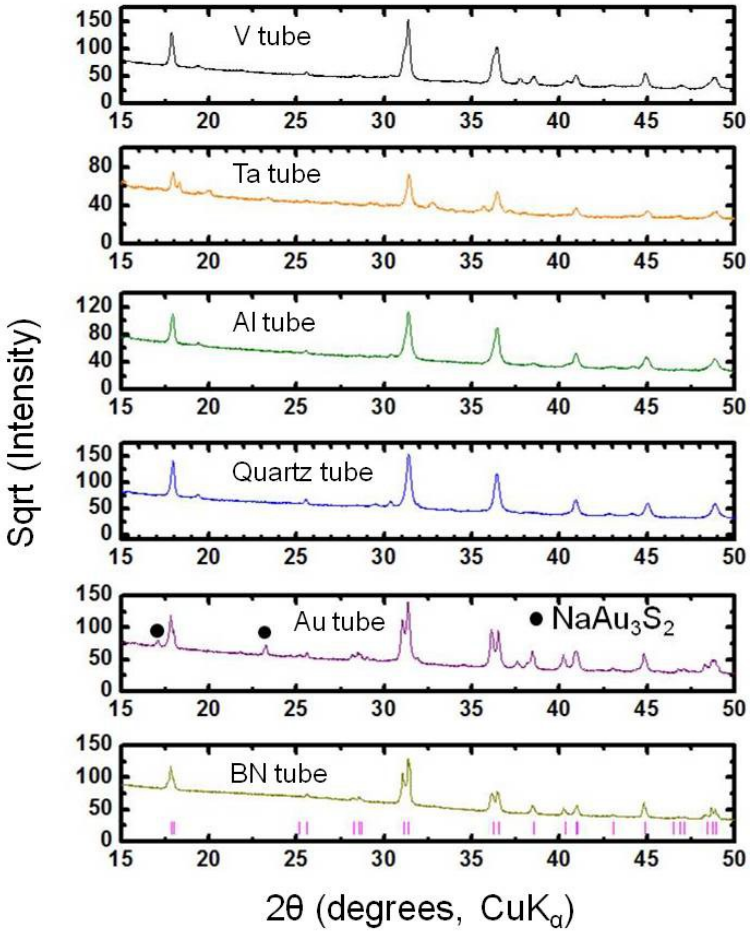

Figure 4. Diffraction patterns of the as-prepared Na_3PS_4 samples which were synthesized at 500 °C with the use of different reaction vessels. The tetragonal phase was produced using boron nitride, or gold tubes. The cubic phase was produced using quartz, aluminum or tantalum tubes, although unknown impurities are present in the product prepared with tantalum tubes. Use of vanadium tubes produces the high-temperature tetragonal phase whose lattice parameters are close to that of the cubic polymorph. For clarity, only tick marks corresponding to the tetragonal lattice are shown in the bottom panel. The square root of intensity is plotted on the *y* axis.

The cubic Na_3PS_4 can be prepared at 500 °C with the use of either quartz or Al tubes. We have therefore performed a final test by using Al or quartz tubes, but with different amounts of precursors. As shown in Fig. 5, when less than 0.1 g of precursors is used, the cubic phase can be produced. However, when more than 0.3 g of precursors is used, the tetragonal polymorph is produced (evidenced by the peak splitting at approximately 36.5°).

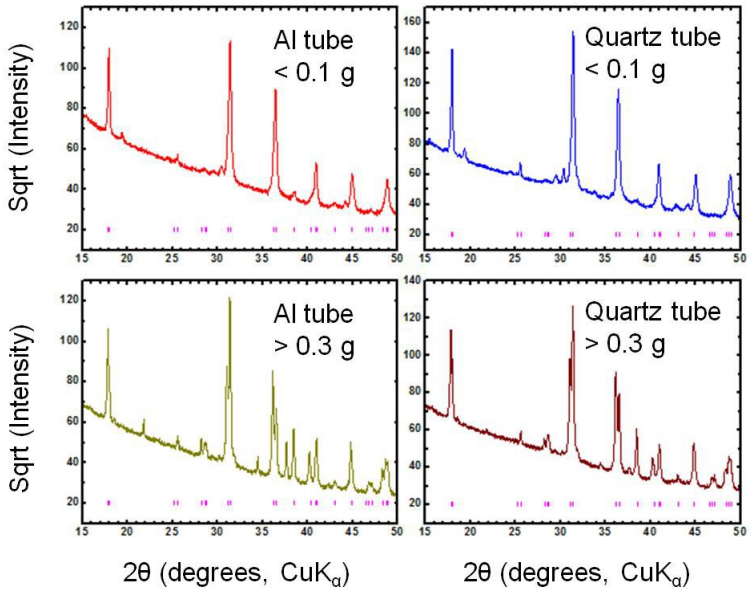

Figure 5. Diffraction patterns of the as-prepared Na_3PS_4 samples synthesized at 500 °C with the use of Al or quartz tubes, and with different amounts of precursors. The cubic phase is only formed when the mass of the precursors is below 0.1 g. Tick marks corresponding to the tetragonal lattice are shown in all panels. The square root of intensity is plotted on the *y* axis.

Syntheses and structural characterizations of $Na_3PS_xSe_{4-x}$

We have prepared the solid solution phases (x = 1, 2, 3), to fully characterize their structures and understand the impact of compositions on Na-ion conduction. The diffraction patterns of these phases, together with the two end members (*i.e.*, Na_3PS_4 and Na_3PSe_4) are shown in Fig. 6. With increasing Se content, a gradual peak shift toward lower angle is observed. This systematic peak shift suggests a gradual volume expansion from the S-rich to Se-rich compositions, which is consistent with the replacement of the smaller S^{2-} anions with the larger Se^{2-} anions. Also of note is that the peak splitting associated with the tetragonal polymorph is present in the x = 4 sample, less apparent in the x =3 sample, and becomes absent in the x= 0, 1, and 2 samples, suggesting a tetragonal-to-cubic structural transition with increasing Se content.

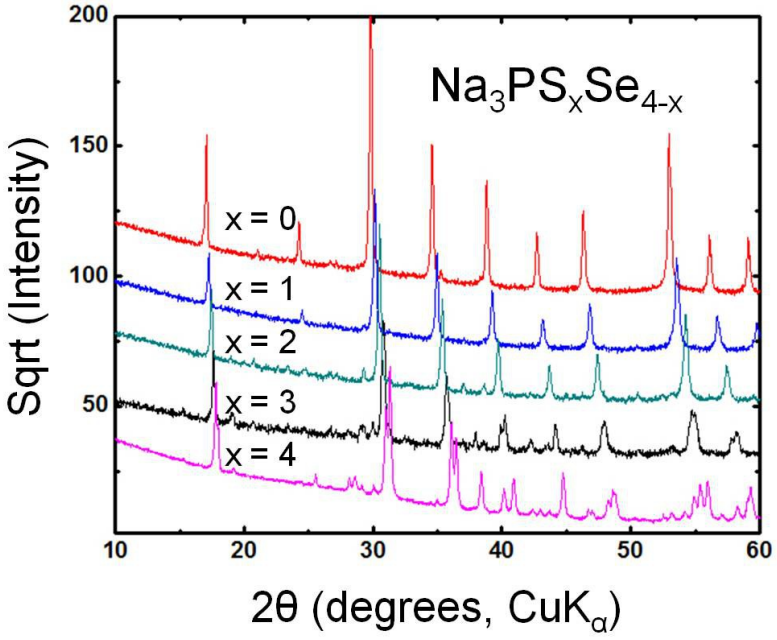

Figure 6. Diffraction patterns of the $Na_3PS_xSe_{4-x}$ phases.

A careful structural characterization for these phases was subsequently performed through Rietveld refinements of the synchrotron X-ray diffraction data. The much higher resolution (d_{min} ~ 0.6 Å) and much better counting statistics (or signal-to-noise ratio) of the synchrotron XRD data compared with the laboratory data allowed us to accurately determine the structures of $Na_3PS_xSe_{4-x}$ phases, as well as to identify the minor impurities that are present but not visible in the laboratory XRD data. We determined the tetragonal symmetry of the x = 3 and 4 phases, and the cubic symmetry of the x = 1 and 2 phases. The minor impurity phases that are present in each sample are tabulated in Table 1. We observed ~1 wt% Na_2S_2 in the x =4 sample, ~5 wt% NaS_2 in the x = 3 sample, ~6 wt% $NaSe_2$ and ~2 wt% NaS_2 in the x = 2 sample, ~2 wt% $NaSe_2$ in the x = 1 sample.

Table 1. Weight fractions of phases present in the $Na_3PS_xSe_{4-x}$ samples from Rietveld refinement results.

Composition	Phase fraction (wt%)
Na_3PS_4 (or x = 4)	93.34(5)% Na_3PS_4, 5.82(2)% Na_3POS_3, 0.84(2) % Na_2S_2
Na_3PS_3Se (or x = 3)	80.4(3)% Na_3PS_3Se, 8.2(2)% Na_3POS_3, 6.3(2)% Na_3POS_2Se, 5.1(1)% $NaSe_2$
$Na_3PS_2Se_2$ (or x = 2)	91.4(2)% $Na_3PS_2Se_2$, 6.07(6)% $NaSe_2$, 1.9(2)% NaS_2, 0.7(1)% black phosphorus
Na_3PSSe_3 (or x = 1)	98.30(3)% Na_3PSSe_3, 1.71(3)% $NaSe_2$

The final refinements were carried out by incorporating all the minor impurities, and by constraining the compositions of these compounds to the nominal stoichiometry. The refinement

results are presented in Fig. 7 (the data for Na_3PSe_4 has been reported in a separate work[12]). The structural parameters for Na_3PS_3Se, $Na_3PS_2Se_2$ and Na_3PSSe_3 are listed in Table S1-S6 of the Supporting information. The refined cell volume of the $Na_3PS_xSe_{4-x}$ phases expands in nearly linear fashion with increasing Se concentration (Fig. 8). The same trend was also observed for the Na - S/Se and P - S/Se bond lengths. Tanibata *et. al* observed that approximately 20% Na occupies an interstitial Na site in a 6% Si doped Na_3PS_4 sample on the basis of laboratory XRD data [15]. Similarly, Zhang *et. al.* also observed interstitial Na in cubic Na_3PSe_4 through Fourier difference map [14]. However, when we included interstitial Na in the $Na_3PS_xSe_{4-x}$ structural models, the quality of the fit only marginally increases (*e.g.*, R_{wp} with and without Na interstitial in Na_3PSe_4 are 10.34 and 10.37, respectively). This result does not indicate a substantial presence of interstitial Na in the cubic $Na_3PS_xSe_{4-x}$ structures.

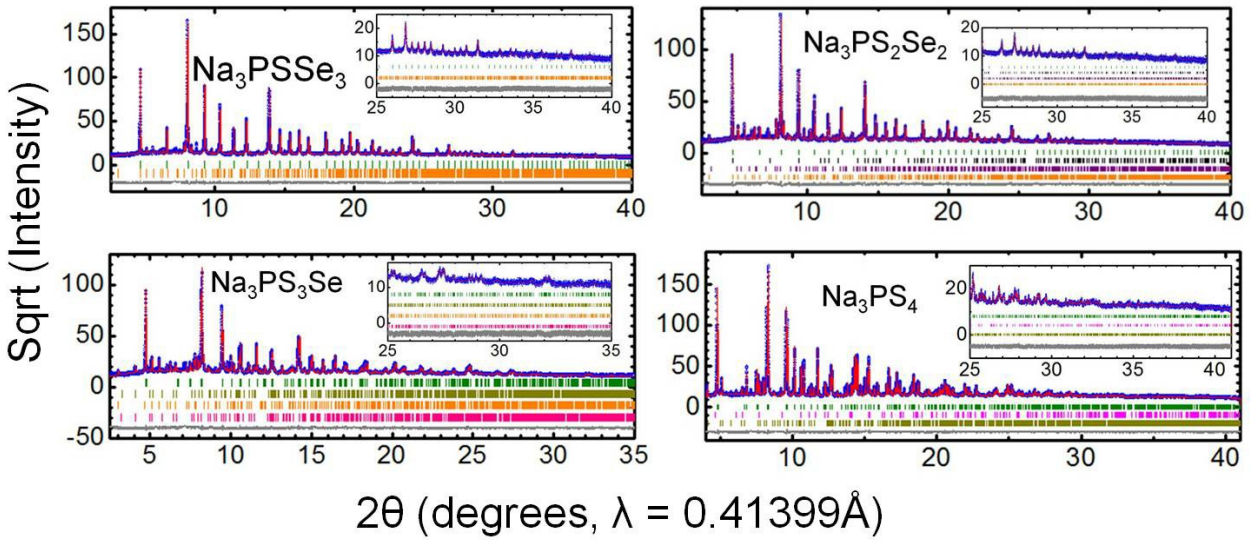

Figure 7. Rietveld refinements of the synchrotron XRD patterns for Na_3PS_4, Na_3PS_3Se, $Na_3PS_2Se_2$ and Na_3PSSe_3. Data were collected at beamline 11 BM of the Advanced Photon Source, Argonne National Laboratory, with a wavelength of 0.41399 Å. The square root of intensity is plotted on the *y* axis. The observed, calculated, and difference curves are shown in blue, red and dark grey, respectively. Reflections corresponding to $Na_3PS_xSe_{4-x}$ (olive), Na_3POS_3 (dark yellow), Na_2S_2 (magenta), Na_3POS_2Se (isostructural to Na_3POS_3, pink), $NaSe_2$ (orange), NaS_2 (purple), and black phosphorus (black) are shown with tick marks of different colors.

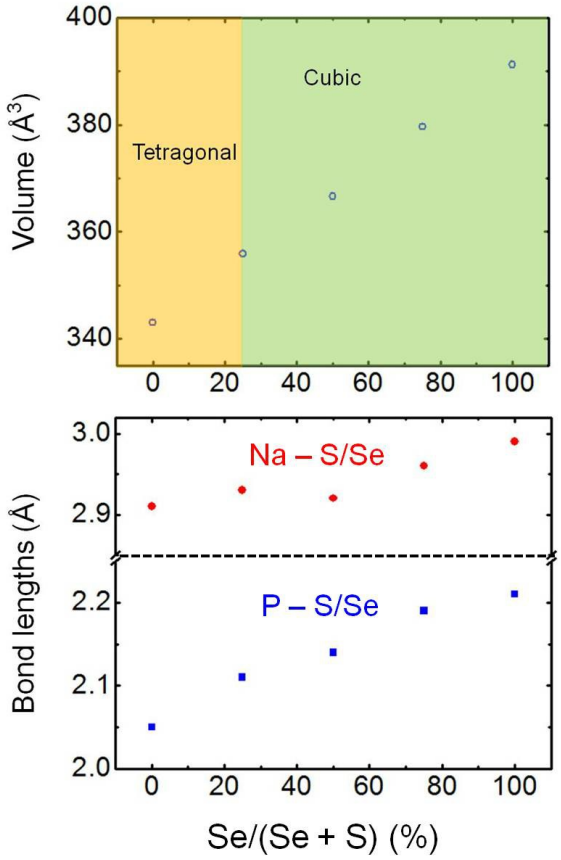

Figure 8. Cell volume (top) and selected bond lengths (Na-S/Se and P-S/Se) *versus* Se concentration. The yellow and green shaded regions as shown in the top panel indicate the compositional ranges where $Na_3PS_xSe_{4-x}$ crystallizes in the tetragonal and cubic structures, respectively.

Na^+ conduction in $Na_3PS_xSe_{4-x}$

Na^+ conductivity in $Na_3PS_xSe_{4-x}$ was evaluated through impedance spectroscopy at selected temperatures under Argon protection. Impedance data were collected during both the heating and cooling cycles (Fig. S1). Diffraction data were also collected before and after the impedance measurements, to confirm that no other side reactions or irreversible changes had

occurred to the sample (Fig. S2). Indeed, the diffraction patterns for the $Na_3PS_xSe_{4-x}$ powder samples before and after the variable-temperature impedance measurements (Fig. S2) exhibit the same set of peaks. However, similar to our previous observation in Na_3PSe_4 [12], we observed a noticeable peak width increase for the diffraction patterns of the $Na_3PS_xSe_{4-x}$ powder samples after pressing. A further diffraction study on the Na_3PS_4 samples which were pressed at various pressures establishes a positive correlation between peak width and processing pressure (Fig. S3). Based on a full-profile fitting, this increased peak width is primarily due to an increase in strain. Therefore, we conclude that the irreversible strain development after mechanical pressing is not unique to selenides, but also occurs in sulfides, indicating a general phenomenon for "soft" materials. However, the physical nature of the strain and the possible impact of strain development on the ionic diffusion process still remain elusive.

With increasing concentration of Se in the solid solution phases, we observed a gradual decrease in the activation energy for Na^+ diffusion (Fig. 9). The activation energy for Na diffusion was determined to be 52(4) kJ/mol in tetragonal Na_3PS_4, which agrees well with the previous work of Jansen and co-workers [18], and decreases to 27(1) kJ/mol in Na_3PSe_4. The room-temperature ionic conductivity of $Na_3PS_xSe_{4-x}$ appears to increase with increasing Se concentration, except that the conductivity of Na_3PS_3Se is lower than that of Na_3PS_4. Noting that different amounts of impurity phases, as observed in the synchrotron XRD data, are present in these samples, the observed conductivity variation may not be intrinsically correlated with compositional difference. It should be also noted that the room-temperature conductivity of $Na_3PS_2Se_2$ and Na_3PSe_4 reported in a recent work by Zhang and co-workers [14] is higher than the values obtained in the current study. Different precursors, reaction vessels and temperatures were used in Zhang's work [14]. They also used an additional ball milling step before the impedance

measurements. These differences can cause a change in stoichiometry, a reduction in particle size, and/or an increase in lattice strain of the sample, all of which could affect the ionic diffusion process. Such differences in conductivity from different preparations are not uncommon in not fully optimized ionic conductors.

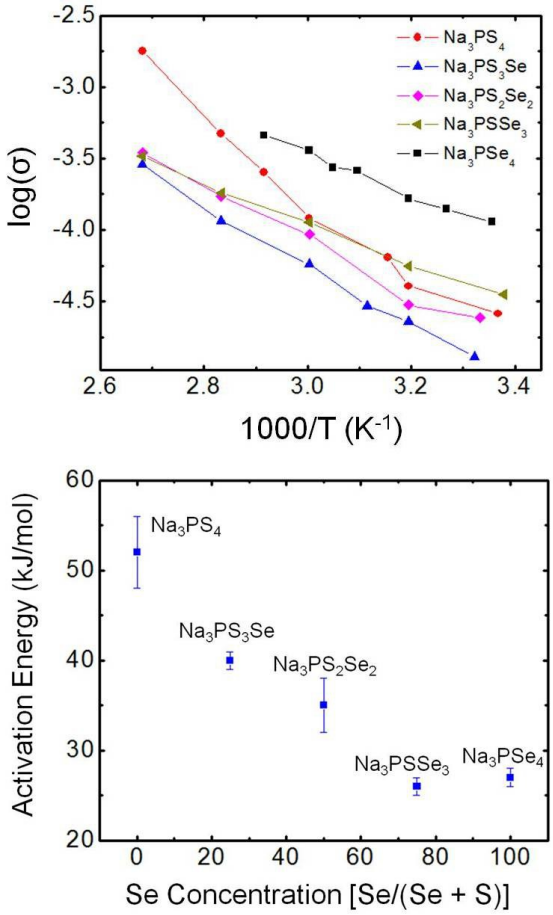

Figure 9. The conductivity (S/cm) vs. temperature plots for $Na_3PS_xSe_{4-x}$ (x= 0, 1, 2, 3, 4) are displayed on the top panel. The conductivity data for Na_3PSe_4 is taken from ref 12. The bottom panel compares the activation energy for Na^+ diffusion as a function of Se concentration.

Discussion

Tetragonal-to-cubic phase transition

The DFT computed energies of the cubic and tetragonal $Na_3PS_xSe_{4-x}$ are listed in Table 2. For $Na_3PS_xSe_{4-x}$ with x=1, 2 and 3, all possible configurations (3, 6 and 3 configurations for x = 1, 2 and 3) of anion (S/Se) ordering in the unit-cell (containing 16 atoms) are considered, and the calculated result with the lowest total energy for each composition is presented.

As shown in Table. 2, the energy of the cubic Na_3PS_4 was calculated to be 44.8 meV/f.u. (or 5.6 meV/atom) higher than the tetragonal structure, consistent with a recent computational work by Ong *et. al* [17]. This energy difference is substantially reduced in Se-containing compositions, suggesting that the stability of the cubic (or tetragonal) polymorph in $Na_3PS_xSe_{4-x}$ can be modulated through compositional tuning. For $Na_3PS_xSe_{4-x}$ with $x \leq 2$, the energy difference between the cubic and tetragonal polymorphs becomes very close to zero. Therefore, it is likely that entropy contributions can stabilize the cubic polymorph at room temperature and above.

Table 2. Calculated phase stability at 0 K for $Na_3PS_xSe_{4-x}$ in the cubic and tetragonal polymorphs.

Composition	Type	Energy above the hull
Na_3PS_4	tetragonal	0 meV/atom 0 meV/f.u.
	cubic	5.6 meV/atom 44.8 meV/f.u.
Na_3PS_3Se	tetragonal	2.3 meV/atom 18.4 meV/f.u.
	cubic	4.9 meV/atom 39.2 meV/f.u.
$Na_3PS_2Se_2$	tetragonal	3.5 meV/atom 24.0 meV/f.u.
	cubic	2.7 meV/atom 21.6 meV/f.u.
Na_3PSSe_3	tetragonal	1.8 meV/atom 14.4 meV/f.u.
	cubic	2.1 meV/atom 16.8 meV/f.u.
Na_3PSe_4	tetragonal	0 meV/atom 0 meV/f.u.
	cubic	0.8 meV/atom 6.4 meV/f.u.

S/Se anion ordering

We observed no anion ordering between S and Se, since no diffraction peaks associated with such superstructures are present (Fig. 7). This is in contrast to the long-range ordering observed in the mixed system of $Na_3PO_xS_{4-x}$. The larger ionic size difference between O^{2-} and S^{2-} creates heavily distorted $PO_xS_{4-x}^{3-}$ tetrahedra and long range ordering related to the orientations of the $PO_xS_{4-x}^{3-}$ tetrahedra [26-28]. While the same local distortion of $PS_xSe_{4-x}^{3-}$ tetrahedra is expected to be present in $Na_3PS_xSe_{4-x}$, the smaller size difference between S^{2-} and Se^{2-} does not create a strong enough interaction to cause long-range ordering of these $PS_xSe_{4-x}^{3-}$ tetrahedra. Our calculations

show a slight energy increase by switching from $PS_2Se_2^{3-}$ groups in $Na_3PS_2Se_2$ to equally populated $PS_4^{3-}$and PSe_4^{3-} groups (~2 kJ/mol). Hence, a variety of local environments (*i.e.*, PS_4^{3-}, PSe_4^{3-} and $PS_xSe_{4-x}^{3-}$) may be present.

Stabilization of the metastable cubic Na_3PS_4

The stabilization of the metastable cubic Na_3PS_4 cannot be explained through entropy contributions only. The use of different reaction tubes produced different polymorphs of Na_3PS_4 (Fig. 4). Even variations of the amount of precursors in the same tube (such as Al or quartz tubes) led to the formation of different polymorphs (Fig. 5). These results indicate that the formation of cubic Na_3PS_4 is very likely induced by the precursors reacting with the tubes. Furthermore, the amount of impurities which can be incorporated into Na_3PS_4 from the tube determines if the less defective tetragonal polymorph (less impurity incorporation) or the more defective cubic polymorph is formed. Different scenarios under which the reaction between the tube and the precursors impacts the products are possible. Elements from the tube may be doped into the structure of Na_3PS_4. Alternatively, off-stoichiometry may be induced in the system by consumption of some precursors through reaction with the tube. The latter is more likely, since aliovalent doping (such as the replacement of P^{5+} with Si^{4+}) appears to be not energetically favorable [17].

Role of defects in Na^+ conduction

Our previous study suggested the key role of defects in enabling fast Na^+ conduction in the structural framework of cubic Na_3PSe_4 [12]. In AIMD simulations, we observed that Na ions in stoichiometric Na_3PSe_4, either in the tetragonal or the cubic structure, were almost immobile. When a small concentration of defects are introduced (*e.g.*, 2.1% Na vacancy), Na^+ conduction in both the tetragonal and cubic phases becomes extremely facile. The same scenario actually occurs in Na_3PS_4 as well. When 2.1 % Na vacancies are introduced into the tetragonal and cubic structures, the activation energy for Na^+ diffusion is approximately 10 kJ/mol for the tetragonal phase and 8 kJ/mol for the cubic phase (Fig. 10). Also, the simulated Na-ion diffusivity is almost the same at the same temperature even for different compositions (Na_3PS_4 and Na_3PSe_4) and polymorphs (cubic and tetragonal). When approximately 6% interstitial Na was introduced into cubic Na_3PS_4, Zhu and co-workers calculated the activation energy for Na-ion diffusion in cubic Na_3PS_4 to be 25 kJ/mol [17]. These results indicate that the fast Na^+ conduction in $Na_3PS_xSe_{4-x}$ is not necessarily correlated with the specific polymorph (*i.e.*, tetragonal or cubic), and instead, is determined by the presence of defects (*e.g.*, Na vacancy or interstitial Na). Hence, the lattice symmetry and composition of Na_3PX_4, and the high Na-ion conductivity may not be causally related. But the symmetry of the Na_3PX_4 polymorph may be related to another feature of the compound, most likely off-stoichiometry and/or impurity doping.

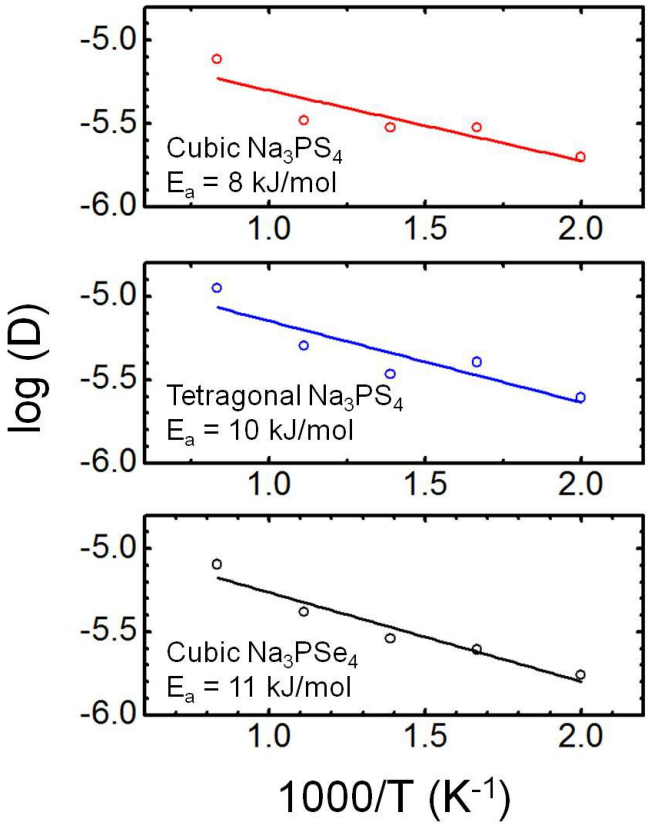

Figure 10. Arrhenius plot of AIMD simulated Na-ion diffusivities (cm^2/s) for cubic and tetragonal Na_3PS_4 with the presence of 2.1% Na vacancy. The diffusivity data of cubic-Na_3PSe_4 with the same amount of Na vacancy from ref. 12 are also shown for comparison.

Since stoichiometric cubic Na_3PX_4 were calculated to be poor Na-ion conductors, we propose that the presence of Na vacancies in cubic Na_3PX_4 is responsible for the high conductivity observed experimentally. Na vacancy was found to be the most plausible defect in cubic Na_3PSe_4 [12]. In this study we calculated the phase stability and defect formation energy for both cubic and tetragonal Na_3PX_4 (X=S, Se) with Na vacancies. The results of our calculations are listed in Table 3. The Na vacancy formation energy for cubic Na_3PS_4 obtained in this study is significantly lower than that of aliovalent dopants considered in another recent work [17]. We note

that the defect formation energy in each polymorph is referenced to the energy of its pristine phase (*e.g.*, the defect formation energy of cubic $Na_{47}P_{16}S_{64}$ is referenced to the energy of cubic Na_3PS_4, not its tetragonal phase). Due to the complexity of anion disorder we did not perform defect calculations for the S/Se mixed phases. However, it is expected that the defect formation energies for $Na_3PS_xSe_{4-x}$ (x=1,2 and 3) are in between the values of Na_3PS_4 and Na_3PSe_4.

Table 3. Calculated stability and Na vacancy formation energy for $Na_3PS_xSe_{4-x}$ in the cubic and tetragonal polymorphs with Na vacancies.

Composition	Type	Energy above the hull	Vacancy formation energy (eV/defect)
$Na_{47}P_{16}S_{64}$	tetragonal	5.2 meV/atom 41.6 meV/f.u.	0.57
	Cubic	8.3 meV/atom 66.4 meV/f.u.	0.34
$Na_{47}P_{16}Se_{64}$	tetragonal	3.6 meV/atom 28.8 meV/f.u.	0.46
	Cubic	4.1 meV/atom 32.8 meV/f.u.	0.39

The formation of a Na vacancy in $Na_3PS_xSe_{4-x}$ can be charge balanced by partial oxidation of S^{2-} and/or Se^{2-} anions. Although it is difficult to directly prove the oxidation of S^{2-}/Se^{2-} in a sample of $Na_3PS_xSe_{4-x}$, indirect evidence is given by the presence of other impurity phases containing oxidized S^{2-} and/or Se^{2-} anions. The synchrotron XRD data on the solid solution phases identified the presence of minor impurities, such as Na_2S_2, NaS_2 and $NaSe_2$ (Table 1). All these minor impurities possess either S_2^{2-}, S_2^- or Se_2^- anions which are oxidized forms of S^{2-} and Se^{2-}, suggesting that the synthesis condition can stabilize oxidized S^{2-} and Se^{2-} anions. The formation of only Se_2^- but not Se_2^{2-} species is most likely a result of the lower electronegativity of

Se compared to S. At the same chemical potential, as determined by the synthesis conditions, S^{2-} can be oxidized to intermediate oxidation states (such as S_2^{2-}), which, on the other hand, does not occur for Se^{2-}.

Conclusions

In this work, we showed that the synthesis of cubic Na_3PS_4 depends on temperature, reaction vessels, and the amount of precursors, all of which indicate that the cubic phase is related to off-stoichiometry and/or impurity doping from the reaction vessel. We have also prepared a series of $Na_3PS_xSe_{4-x}$ solid solution phases, and have accurately determined their structures from high-resolution synchrotron XRD. A tetragonal-to-cubic phase transition with increasing Se concentration in $Na_3PS_xSe_{4-x}$ was observed, which can be explained by a reduced energy difference between the tetragonal and the cubic structures. Different from the common belief in prior literature, we believe that fast Na-ion diffusion in $Na_3PS_xSe_{4-x}$ is enabled by the presence of defects, most likely Na vacancies, and may not be directly linked with the specific polymorph or composition. Rather, the symmetry of the polymorph and the conductivity may all be correlated to intrinsic or extrinsic compositional variations.

Acknowledgement:

This work was supported by the Samsung Advanced Institute of Technology. Use of the Advanced Photon Source at Argonne National Laboratory was supported by the U. S. Department of Energy, Office of Science, Office of Basic Energy Sciences, under Contract No.

DE-AC02-06CH11357. Computational resources from the National Energy Research Scientific Computing Center (NERSC), a DOE Office of Science User Facility supported by the Office of Science of the U.S. Department of Energy under Contract No. DE-AC02-05CH11231, and from the Extreme Science and Engineering Discovery Environment (XSEDE, which is supported by National Science Foundation grant number ACI-1053575) are gratefully acknowledged.

Notes and References:

1. X. Li, D. Wu, Y.-N. Zhou, L. Liu, X.-Q. Yang and G. Ceder, *Electrochemistry Communications*, 2014, **49**, 51-54.
2. L. Liu, X. Li, S. H. Bo, Y. Wang, H. Chen, N. Twu, D. Wu and G. Ceder, *Advanced Energy Materials*, 2015, **5**.
3. J. Ma, S.-H. Bo, L. Wu, Y. Zhu, C. P. Grey and P. G. Khalifah, *Chemistry of Materials*, 2015, **27**, 2387-2399.
4. B. L. Ellis, W. R. M. Makahnouk, Y. Makimura, K. Toghill and L. F. Nazar, *Nat. Mater.*, 2007, **6**, 749-753.
5. J. Liu, D. Chang, P. Whitfield, Y. Janssen, X. Yu, Y. Zhou, J. Bai, J. Ko, K.-W. Nam and L. Wu, *Chemistry of Materials*, 2014, **26**, 3295-3305.
6. N. Yabuuchi, M. Kajiyama, J. Iwatate, H. Nishikawa, S. Hitomi, R. Okuyama, R. Usui, Y. Yamada and S. Komaba, *Nat. Mater.*, 2012, **11**, 512-517.
7. S. K. Kim, A. Mao, S. Sen and S. Kim, *Chemistry of Materials*, 2014, **26**, 5695-5699.
8. T. J. Udovic, M. Matsuo, A. Unemoto, N. Verdal, V. Stavila, A. V. Skripov, J. J. Rush, H. Takamura and S.-i. Orimo, *Chem. Commun.*, 2014, **50**, 3750-3752.
9. J. T. Kummer, *Progress in solid state chemistry*, 1972, **7**, 141-175.
10. A. K. Kuriakose, T. A. Wheat, A. Ahmad and J. Dirocco, *Journal of the American Ceramic Society*, 1984, **67**, 179-183.
11. W. D. Richards, T. Tsujimura, L. J. Miara, Y. Wang, J. C. Kim, S. P. Ong, I. Uechi, N. Suzuki and G. Ceder, *Nature Communications*, 2016, **7**.
12. S.-H. Bo, Y. Wang, J. C. Kim, W. D. Richards and G. Ceder, *Chemistry of Materials*, 2015, DOI: 10.1021/acs.chemmater.5b04013.
13. A. Hayashi, K. Noi, A. Sakuda and M. Tatsumisago, *Nature communications*, 2012, **3**, 856.
14. L. Zhang, K. Yang, J. Mi, L. Lu, L. Zhao, L. Wang, Y. Li and H. Zeng, *Advanced Energy Materials*, 2015, DOI: 10.1002/aenm.201501294, n/a-n/a.
15. N. Tanibata, K. Noi, A. Hayashi, N. Kitamura, Y. Idemoto and M. Tatsumisago, *Chemelectrochem*, 2014, **1**, 1130-1132.
16. Y. Wang, W. D. Richards, S. P. Ong, L. J. Miara, J. C. Kim, Y. Mo and G. Ceder, *Nat Mater*, 2015, **14**, 1026-1031.
17. Z. Zhu, I.-H. Chu, Z. Deng and S. P. Ong, *Chemistry of Materials*, 2015, DOI: 10.1021/acs.chemmater.5b03656.

18. M. Jansen and U. Henseler, *J Solid State Chem*, 1992, **99**, 110-119.
19. J. P. Perdew, K. Burke and M. Ernzerhof, *Physical review letters*, 1996, **77**, 3865.
20. P. E. Blöchl, *Phys Rev B*, 1994, **50**, 17953.
21. G. Kresse and J. Furthmüller, *Phys Rev B*, 1996, **54**, 11169.
22. *Inorganic Crystal Structure Database (FIZ Karlsruhe, 2014); http://icsd.fiz-karlsruhe.de/icsd*
23. G. Hautier, C. Fischer, V. Ehrlacher, A. Jain and G. Ceder, *Inorg. Chem.*, 2010, **50**, 656-663.
24. L. J. Miara, W. D. Richards, Y. E. Wang and G. Ceder, *Chemistry of Materials*, 2015.
25. S. P. Ong, W. D. Richards, A. Jain, G. Hautier, M. Kocher, S. Cholia, D. Gunter, V. L. Chevrier, K. A. Persson and G. Ceder, *Comp Mater Sci*, 2013, **68**, 314-319.
26. M. Pompetzki and M. Jansen, *Zeitschrift für anorganische und allgemeine Chemie*, 2002, **628**, 641-646.
27. M. Pompetzki, R. E. Dinnebier and M. Jansen, *Solid state sciences*, 2003, **5**, 1439-1444.
28. M. Pompetzki and M. Jansen, *ChemInform*, 2004, **35**.

TOC:

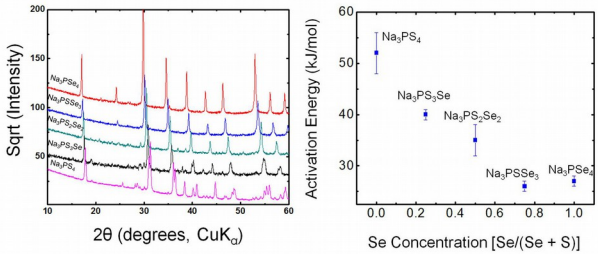

Fast Na-ion diffusion in $Na_3PS_xSe_{4-x}$ may not be causally related with the symmetry of the polymorph, but with compositional variations.